

Shell-type micromechanical actuator and resonator

Maxim Zalalutdinov,^{a)} Keith L. Aubin, Robert B. Reichenbach, Alan T. Zehnder, Brian Houston, Jeevak M. Parpia, and Harold G. Craighead

*Cornell Center for Material Research, Cornell University, Ithaca, New York 14853-2501
and Naval Research Laboratory, 4555 Overlook Avenue SW, Washington, DC 20375*

(Received 1 May 2003; accepted 2 September 2003)

Dome-shaped radio-frequency micromechanical resonators were fabricated by utilizing the buckling of a prestressed thin polysilicon film. The enhanced rigidity of the dome structure leads to a significant increase of its resonant frequency compared to a flat plate resonator. The shell-type geometry of the structure also provides an imbedded actuation mechanism. Significant out-of-plane deflections are actuated by mechanical stress introduced within the plane of the shell. We demonstrate that thermomechanical stress generated by a focused laser beam, or microfabricated resistive heater, provides an effective and fast mechanism to operate the dome as an acoustic resonator in the radio-frequency range. All-optical operation of the shell resonator and an integrated approach are discussed. © 2003 American Institute of Physics. [DOI: 10.1063/1.1622792]

High-frequency microelectromechanical systems (MEMS) are widely considered as an element base for signal processing in the next generation of wireless communication devices.^{1–3} Parametric amplification,^{4,5} limit cycle oscillations,⁶ and injection locking⁷ demonstrated for MEMS oscillators allows one to build active circuits where signal processing would be implemented in the mechanical domain. However, a transduction mechanism for the effective conversion between the electrical and mechanical forms of the signal remains one of the key problems in MEMS design. The widely used capacitive drive⁸ imposes restrictions related to cross talk issues and to high voltages required for actuation. Piezoelectric⁹ or magnetomotive¹⁰ actuation cannot be readily integrated because of the requirement for integrated circuit (IC)-incompatible materials or high magnetic fields.

In this letter, we demonstrate a design for a rf MEMS resonator based on the geometry of a shallow segment of a thin spherical shell. The finite curvature of the shell introduces an imbedded actuation mechanism by coupling the in-plane stress to the out-of-plane deflection of the shell.¹¹ The key feature of the shell actuation mechanism described in this letter is the local nature of the driving stress introduced at a specific point of the shell. A similar approach is employed in the design of macroscopic induced-strain actuators,^{12,13} for “smart structures” actuated by small piezoelectric patches, surface bonded on a cylindrical shell at certain locations.

In our micromechanical shell actuator, the in-plane strain is provided by stress introduced directly inside the shell layer. In our experiments we employ thermoelastic stress created by heating of the shell either by using a focused laser beam or a microfabricated heater. Using local heating, one can actuate cantilevering shell or bowl-type structures (shells supported at the center point). In the latter case, the compressive stress applied in the hoop direction close to the free edge of the shell flattens the bowl and provides a vertical component to the deflection of the periphery. The resulting motion can be complicated; thus for the configuration considered in this letter—a dome-shaped structure (shell clamped at the

periphery)—we employ finite element analysis (FEA) to demonstrate that nonhomogeneous stress provides significant distortion of the shape (see Fig. 1).

The fact that spatial temperature variation can cause significant bending moments¹⁴ and vibrations¹⁵ is known from models of macroscopic panels. The key difference is that the period of the thermally induced vibrations for the macroscopic plates is determined by the thermal relaxation time. In MEMS structures, the small thermal mass makes the shell cooling time comparable to the period of the transverse vibrations. We have demonstrated that when the driving local stress is modulated at the fundamental frequency of the mechanical vibrations of the dome, a large amplitude standing wave pattern is created, transforming the shell into a high-frequency acoustic resonator.

The fabrication process for the dome-type resonators described in this letter was based on a buckling phenomenon. The device layer, a 200 nm thick polysilicon film, was grown using low-pressure chemical vapor deposition (LPCVD) on top of the sacrificial SiO₂ layer (thickness 1560 nm) thermally grown over a silicon wafer. The parameters of the LPCVD process (temperature 570 °C, rate 3 nm/min) and subsequent thermal annealing (1150 °C, 1 h) were chosen to provide significant compressive stress inside the resulting polysilicon layer.¹⁶ The final measurements, based on a substrate bending principle,¹⁷ indicate the presence of compressive stress in excess of 220 MPa.

Optical lithography and a chlorine-based reactive ion etch were used to open 4 μm diameter holes in the top polysilicon layer. Submersing the wafer in hydrofluoric acid (HF, 49%) undercuts the sacrificial oxide layer surrounding the holes, resulting in a suspended annular disk structure that is free on the inside and clamped at the periphery. The released disk is compressed and an estimate based on the theory of elastic stability¹⁸ shows that buckling should occur when the radius of the undercut exceeds 6 μm (calculated for the built-in stress and thickness of our film). The asymmetry of the real system in the vertical direction may provide earlier buckling¹⁹ and also leads to preferential upbuckling, preventing the released membrane from snapping into the substrate. The total timing of the wet etch determines the outer diam-

^{a)}Electronic mail: maxim@ccmr.cornell.edu

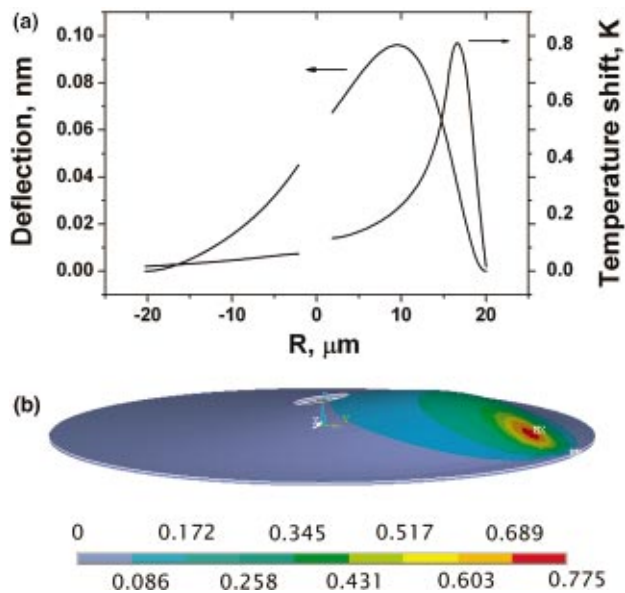


FIG. 1. (Color) Results of FEA calculations for the temperature profile ΔT and deflection δu of the dome, caused by the concentrated heat load ($P_{\text{heating}} = 100 \mu\text{W}$) located at the edge of the dome. ΔT and δu are plotted along the diameter crossing the heating spot (a). Color code on the three-dimensional image of the distorted dome shape corresponds to the change of local temperature in Kelvin (b).

eter of the shell. Figure 2 shows an optical image of the 40 μm diameter polysilicon dome obtained using the differential interference contrast (DIC) technique. The interferometric circles observed using the coherent light illumination give an estimate ($h \sim 1 \mu\text{m}$) for the dome height.

The resulting dome structures are robust enough to withstand the next lithography step. Resistive heaters were microfabricated on the face of the domes using photolithography with image reversal²⁰ and lift-off process. Figure 3(b) illustrates a dome with a 6 μm wide meander metal heater (resistivity $R_{\text{heater}} = 6 \Omega/\square$, 20 nm gold on 10 nm titanium adhesion layer) deposited using an electron-beam evaporation technique.

The vertical motion of the surface of the shell was detected interferometrically²¹ by measuring the variation of the intensity of a red HeNe laser beam reflected by the dome. Using a XYZ micropositioning system and an optical micro-

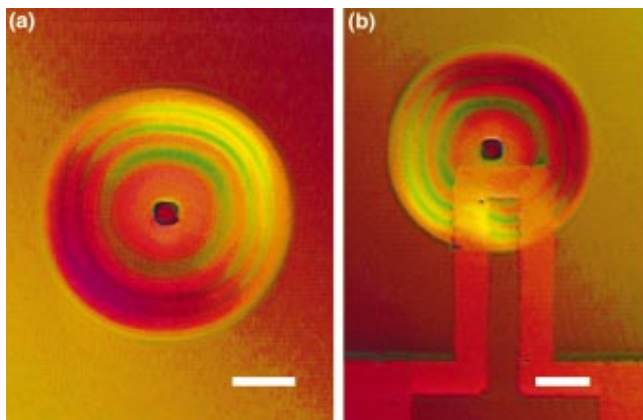


FIG. 2. (Color) Optical DIC image of a polysilicon dome resonator, radius $R = 20 \mu\text{m}$, thickness $b = 200 \text{ nm}$, apex rise $h \sim 900 \text{ nm}$ (a). A dome resonator (same dimensions) with microfabricated resistive heater (b). Scale bars correspond to 10 μm .

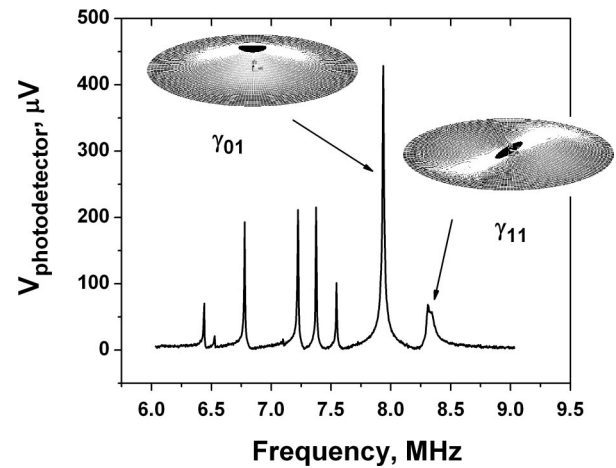


FIG. 3. Spectrum of the fundamental modes of the bare dome resonator acquired using Ar^+ laser drive and interferometric (HeNe laser) detection (all-optical operation). The modes of vibrations (see insets) were identified by varying the relative positions of the two laser beams and analyzing the spatial pattern of the phase difference between the driving signal and the detected mechanical motion. Multiple peaks corresponding to identical modes of vibrations but with different spatial orientation are observed due to slight asymmetry in the geometry of the dome. The highest quality factor ($Q \sim 10\,000$) was exhibited by the γ_{01} mode.

scope, the 5 μm diameter laser spot can be located at any place of interest on the shell. A second laser beam (blue 450 nm Ar^+ -ion laser) with an electro-optical modulator (bandwidth $\leq 80 \text{ MHz}$) was added to the experimental setup to actuate the dome resonator. The blue laser was focused on the device under test by the same objective lens. A system of mirrors provided independent positioning of the red and blue laser spots. A dispersing prism or low-pass optical filters were used to prevent the saturation of the photodetector by the reflected blue laser beam.

Figure 1 demonstrates the result of FEA simulations for shape distortion and temperature distribution (color code) over the 40 μm diameter dome generated by a 100 μW , dc, 5 μm diameter heat source at the periphery of the structure. The maximum displacement recorded corresponds to a dc actuation coefficient $\sim 1 \mu\text{m}/\text{W}$. For a high-frequency excitation, the thermoelastic drive can only be effective if the thermal relaxation time T_{relax} is comparable to the period of mechanical vibrations. A cooling rate, $T \propto T_0 e^{-\lambda t}$, for a circular plate with fixed boundary conditions is determined²² by

$$\lambda = \frac{K}{C\rho} \left(\frac{\mu_1^{(0)}}{R} \right)^2, \quad (1)$$

where K is thermal conductivity, C is the heat capacity, ρ is the density, R is the radius of the plate, and $\mu_1^{(0)} = 2.4$ is the root of a Bessel function $J_0(\mu_1^{(0)}) = 0$. For our dome resonator, $T_{\text{relax}} = 1/\lambda \sim 0.7 \mu\text{s}$ enables thermal actuation at a MHz frequency range. It is important to mention that by scaling down the dimensions of the resonator, the resonant frequency increases as b/R^2 (b —film thickness) while λ decreases as R^{-2} making the thermoelastic drive even more effective for smaller devices.

A typical spectrum of a bare (no resistive heater) 40 μm diameter dome obtained using the laser drive ($P_{\text{modulated}}^{\text{laser}} = 30 \mu\text{W}$) is presented in Fig. 3. Different devices, fabricated in a single run demonstrate the position of the resonant

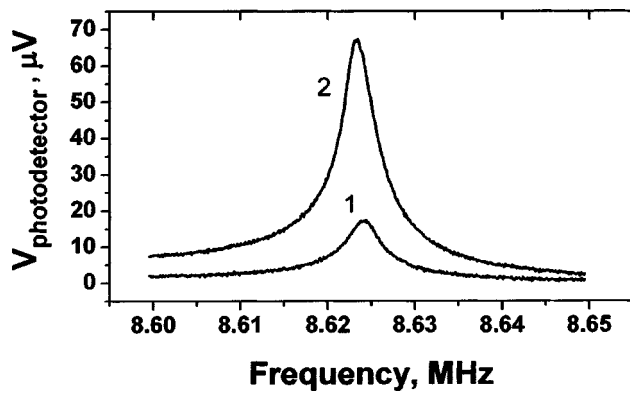


FIG. 4. Resonant peak corresponding to the γ_{01} mode of the vibrations of the dome acquired by microheater actuation with ac excitation power $P_{ac} = 10 \mu\text{W}$ and dc power offset $P_{dc} = 12 \mu\text{W}$ for resonance 1 and $P_{dc} = 200 \mu\text{W}$ for resonance 2. Peak shift caused by dc heating corresponds to the tuning rate $-3 \text{ Hz}/\mu\text{W}$.

peaks consistent within 0.5%. The peaks corresponding to the axisymmetric mode (γ_{01}) and the mode with one diametrical nodal line (γ_{11}), respectively, are located at 7.9 MHz and 8.3 MHz. These values for the domes resonant frequencies are significantly higher than those of an equivalently sized flat annular disk. The extra rigidity of the shell structure comes from the membrane component and can be approximated²³ as

$$\omega_{ij}^{\text{shallow spherical shell}} = \left(\omega_{ij}^{\text{flat plate}} + \frac{E}{\rho\chi^2} \right)^{1/2}, \quad (2)$$

where E is the modulus of elasticity, ρ is the material density, and χ is the curvature radius to the midsurface of the shell segment. Calculations based on Eq. (2) (40 μm diameter dome, thickness 200 nm, γ_{01} mode) with estimated²⁴ $\omega_{\text{flat plate}} \sim 2 \text{ MHz}$ lead to $\omega_{\text{shell}} \sim 6.5 \text{ MHz}$, close to experimentally observed values. We would like to emphasize that buckling is by no means the only method to fabricate shell-type resonators, but is probably the simplest one. Deposition of the shell material on a precurved sacrificial layer could be used to increase the curvature of the dome and further enhance the resonant frequency.

The enhancement of the resonant frequency provided by the shell-type geometry can be crucial for MEMS resonators dedicated for use in rf front-end circuits. The extra rigidity gained without reducing lateral dimensions can significantly expand the frequency range for a given lithography process. To prove that shell-type MEMS can be employed in ICs, we have demonstrated electrical actuation of our dome resonators with microfabricated heaters. The output of a tracking generator of a network analyzer with an added dc component P_{dc} was applied to the microheater, providing high-frequency temperature (and hence stress) modulation. Figure 4 demonstrates a resonance peak acquired using the resistive heater drive. A partial deterioration of the quality factor ($Q_{\text{resistive}} \sim 2500$) caused by the metallic heater could be a reasonable tradeoff for integration. The resonant frequency can be fine tuned by adjusting P_{dc} .

In conclusion, we would like to mention that photoinduced stress, magnetostriction, or the shape-memory mechanism could be used as an alternative to thermoelastic actua-

tion. A dc, or low-frequency, actuator based on the shell geometry is feasible but would require specific applications. Operating the micromechanical shell structure as an acoustic resonator by modulating the applied stress provides the major advantages of low excitation power and extended frequency range. All-optical operation of a shell resonator, described in this letter, can be utilized in sensing applications with an enclosed testing volume. Design of a dome resonator, which would combine low power, low voltage, thermal-resistive actuation with capacitive detection of the mechanical motion, is currently in progress. Such an all-electric device, compatible with complementary metal-oxide-semiconductor technology is expected to have a wide range of applications in rf signal processing.

The authors are grateful to Dan Rugar (IBM) for the discussion that triggered this research and to Bojan Ilic and David Czaplewski for help with fabrication. This work was supported by the Cornell Center for Material Research (CCMR), a Materials Research Science and Engineering Center of the NSF (DMR-0079992). Particular acknowledgment is made for the use of the Cornell Nanofabrication Facilities (CNF). The authors would also like to acknowledge the Office of Naval Research and DARPA for their support.

¹C. T.-C. Nguyen, *Proceedings of the 2000 International MEMS Workshop (iMEMS'01)*, Singapore, 4–6 July 2001, pp. 21–34.

²B. A. Warneke, M. D. Scott, B. S. Leibovitz, Z. Lixia, C. L. Bellew, J. A. Chediak, J. M. Kahn, B. E. Boser, and K. S. Pister, *Proc. IEEE* **2**, 1510 (2002).

³C. T.-C. Nguyen, *Digest of Papers, Topical Meeting on Silicon Monolithic Integrated Circuits in RF Systems*, 12–14 Sept. 2001, pp. 23–32.

⁴D. Rugar and P. Grutter, *Phys. Rev. Lett.* **67**, 699 (1991).

⁵M. Zalalutdinov, A. Olkhovets, A. Zehnder, B. Ilic, D. Czaplewski, H. G. Craighead, and J. M. Parpia, *Appl. Phys. Lett.* **78**, 3142 (2001).

⁶M. Zalalutdinov, A. Zehnder, A. Olkhovets, S. Turner, L. Sekaric, B. Ilic, D. Czaplewski, J. M. Parpia, and H. G. Craighead, *Appl. Phys. Lett.* **79**, 695 (2001).

⁷M. Zalalutdinov, K. L. Aubin, M. Pandey, A. T. Zehnder, R. H. Rand, H. G. Craighead, and J. M. Parpia *Appl. Phys. Lett.* **83**, 3288 (2003).

⁸S. G. Adams, F. M. Bertsch, K. A. Shaw, P. G. Hartwell, F. C. Moon, and N. C. MacDonald, *J. Micromech. Microeng.* **8**, 15 (1998).

⁹D. F. L. Jenkins, M. J. Cunningham, G. Veln, and D. Remiens, *Sens. Actuators A* **63**, 135 (1997).

¹⁰XMH Huang, C.A. Zorman, M. Meregany, and M. L. Roukes, *Nature (London)* **421**, 496 (2003).

¹¹S. Timoshenko *Theory of Plates and Shells* (McGraw-Hill, New York, 1940), pp. 351 and 450.

¹²Z. Chaudhry, F. Lalande, and C. Rogers, *J. Acoust. Soc. Am.* **97**, 2872 (1995).

¹³F. Lalande, Z. Chaudhry, and C. Rogers, *AIAA J.* **33**, 1300 (1995).

¹⁴W. Soedel, *Sound Vib.* **10**, 12 (1976).

¹⁵A. Tylikowski, *J. Therm. Stresses* **24**, 605 (2001).

¹⁶D. Maier-Schneider, A. Koprululu, S. Ballhausen Holm, and E. Obermeier, *J. Micromech. Microeng.* **6**, 436 (1996).

¹⁷K. N. Tu, J. W. Mayer, and L. C. Feldman, *Electronic Thin Film Science for Electrical Engineers and Material Scientists* (Macmillan, New York, 1992), p. 87.

¹⁸S. Timoshenko and J. Gere, *Theory of Elastic Stability* (McGraw-Hill, 1961), p. 389.

¹⁹S. M. Carr and M. N. Wybourne, *Appl. Phys. Lett.* **82**, 709 (2003).

²⁰D. H. Ziger and J. W. Reightler, *Semicond. Int.* **11**, 200 (1988).

²¹D. Carr and H. Craighead, *J. Vac. Sci. Technol. B* **15**, 2760 (1997).

²²A. Jeffrey, *Advanced Engineering Mathematics* (Academic, New York, 2002), p. 1004.

²³W. Soedel, *J. Sound Vib.* **29**, 457 (1973).

²⁴P. M. Morse and K. U. Ingard, *Theoretical Acoustics* (Princeton University Press, Princeton, NJ, 1986), p. 214.